to formation of *trans*-$Rh(NH_3)_4(H_2O)Cl^{2+}$ with a quantum yield of 0.38 mol/einstein.

The retention of stereochemistry in the photolysis of $Rh(en)_3^{3+}$ to form *cis*-$Rh(en)_2(enH)Cl^{3+}$ and the presence of *trans*-$Rh(en)_2Cl_2^+$ as a secondary photolysis product indicate that the photocatalyzed exchange of Cl^- for enH^+ (second step) is proceeding through an excited-state rearrangement. If a dissociative intermediate is proposed for both the photoanation of *cis*-$Rh(en)_2(enH)Cl^{3+}$ and the photoaquation of *cis*-$Rh(en)_2Cl_2^+$, the five-coordinate intermediate ($Rh(en)_2Cl^{2+}$ in both cases) shows a 100% efficiency toward rearrangement so that the incoming ligand enters trans to Cl. This rearrangement must depend on the presence of the chloro ligand and not the two bidentate ethylenediamine ligands in the five-coordinate intermediate since the photolysis of $Rh(en)_3^{3+}$ leads solely to a cis product.

Acknowledgment. The authors acknowledge the donors of the Petroleum Research Fund, administered by the American Chemical Society, for partial support of this research. The authors also thank Dr. Peter C. Ford, University of California, Santa Barbara, Calif., for helpful discussions and a preprint on the photochemistry of *cis*-$Rh(NH_3)_4Cl_2^+$, and Mr. Tadashi Matsubara, UCSB, for his assistance in the synthesis of $[Rh(en)_2(enH)Cl]Cl_3 \cdot 2H_2O$.

Registry No. *cis*-$[Rh(en)_2(enH)Cl]Cl_3$, 63744-43-4; $[Rh(en)_3]Cl_3$, 14023-02-0; ^{13}C, 14762-74-4.

References and Notes

(1) P. C. Ford, R. E. Hintze, and J. D. Petersen in "Concepts of Inorganic Photochemistry", A. W. Adamson and P. D. Fleischauer, Ed., Wiley, New York, N.Y., 1975, Chapter 5.
(2) P. C. Ford and J. D. Petersen, *Inorg. Chem.*, **14**, 1404 (1975).
(3) J. D. Petersen and P. C. Ford, *J. Phys. Chem.*, **78**, 1144 (1974).
(4) J. D. Petersen, R. J. Watts, and P. C. Ford, *J. Am. Chem. Soc.*, **98**, 3188 (1976).
(5) T. L. Kelly and J. F. Endicott, *J. Phys. Chem.*, **76**, 1937 (1972).
(6) C. Kutal and A. W. Adamson, *Inorg. Chem.*, **12**, 1454 (1973).
(7) S. C. Pyke and R. G. Linck, *J. Am. Chem. Soc.*, **93**, 5281 (1971).
(8) M. T. Gandolfi, M. F. Manfrin, A. Juris, L. Moggi, and V. Balzani, *Inorg. Chem.*, **13**, 1342 (1974).
(9) A. D. Kirk, K. C. Moss, and J. G. Valentin, *Can. J. Chem.*, **49**, 1524 (1971).
(10) J. Sellan and R. Rumfeldt, *Can. J. Chem.*, **54**, 519 (1976).
(11) M. D. Alexander and C. A. Spillert, *Inorg. Chem.*, **9**, 2344 (1970).
(12) S. C. Pyke and R. C. Linck, *Inorg. Chem.*, **10**, 2445 (1971).
(13) M. M. Muir and W.-L. Huang, *Inorg. Chem.*, **12**, 1831 (1973).
(14) J. Sellan and R. Rumfeldt, *Can. J. Chem.*, **54**, 1061 (1976).
(15) R. A. Pribush, R. E. Wright, and A. W. Adamson, *J. Am. Chem. Soc.*, **99**, 2495 (1977).
(16) P. S. Sheridan and A. W. Adamson, *J. Am. Chem. Soc.*, **96**, 3032 (1974).
(17) F. Galsbøl, *Inorg. Synth.*, **12**, 269 (1970).
(18) S. A. Anderson and F. Basolo, *Inorg. Chem.*, **1**, 925 (1962).
(19) (a) C. Burgess and F. R. Hartley, *Inorg. Chim. Acta*, **14**, L37 (1975); (b) J. D. Petersen, F. P. Jakse, and J. V. Paukstelis, submitted for publication in *Inorg. Chim. Acta*.
(20) Small peaks due to unreacted starting material, $Rh(en)_3^{3+}$ (46.36 ppm), and secondary photolysis product, *trans*-$Rh(en)_2Cl_2^+$ (45.68 ppm), are observed in addition to the six peaks of the *cis*-$Rh(en)_2(enH)Cl^{3+}$. These impurities were confirmed by spiking the sample with the two impurities. The two impurity peaks could be removed by computer subtraction techniques using authentic spectra of $Rh(en)_3^{3+}$ and *trans*-$Rh(en)_2Cl_2^+$.
(21) Interchange between the λ and δ confirmations of the bidentate ethylenediamine should be rapid on the NMR time scale and should not result in magnetic nonequivalence due to ring confirmation [see E. J. Corey and J. C. Bailar, Jr., *J. Am. Chem. Soc.*, **81**, 2620 (1959)].
(22) Corrections were made spectroscopically by Gaussian curve shape analysis. Concentrations of *trans*-$Rh(en)_2Cl_2^+$ (5–7%) were determined from a well-defined shoulder at 406 nm while concentrations of $Rh(en)_3^{3+}$ (<2%) were calculated from a very small shoulder on the long-wavelength side of the 277-nm band in the photolysis product.
(23) F. Monacelli, *Inorg. Chim. Acta*, **2**, 263 (1968).
(24) Muir and Huang[13] observed some *trans*-$Rh(en)_2Cl_2^+$ in photolyzed solutions of *cis*-$Rh(en)_2Cl_2^+$ and postulated that cis → trans isomerization of the dichloro species may be the primary photolysis step. A recent ^{13}C NMR study[19b] indicates that the *cis*-$Rh(en)_2Cl_2^+$ used in this study was probably a mixture containing 80% cis isomer and 20% trans isomer.
(25) P. C. Ford, private communication.

Contribution from the Lash Miller Chemistry Laboratory and Erindale College, University of Toronto, Toronto, Ontario, Canada

Rhodium Atom Chemistry. 1. Synthesis and Characterization of Dirhodium, Bis(dioxygen)rhodium, and Mono(dioxygen)rhodium

A. J. LEE HANLAN and GEOFFREY A. OZIN*

Received January 11, 1977 AIC70010Y

Optical spectra from 200 to 900 nm have been obtained for Rh atoms in Ar, Kr, and Xe matrices at 10–12 K and are found to correlate reasonably well with the reported gas-phase atomic transitions. The metal concentration and matrix conditions which favor the dimerization of Rh atoms to Rh_2 molecules are quantitatively assessed using optical spectroscopy. The metal clustering that occurs during the matrix deposition process is analyzed in terms of a simple kinetic theory which enables small metal aggregates to be identified in the presence of atomic species. An earlier report of spectra ascribed to Rh atoms isolated in Ne matrices is shown from this study to be more consistent with a mixture of Rh and Rh_2 dimers. With this background information the cocondensation reactions of Rh atoms with O_2 and O_2/inert gas matrices at 10–12 K are investigated under conditions which favor *mononuclear* complex formation (rhodium cluster–dioxygen complexes constitute the subject of part 2 of this study). The infrared spectra recorded under these circumstances indicate that two dioxygen complexes can be generated. These are established from $^{16}O_2/^{18}O_2$ and $^{16}O_2/^{16}O^{18}O/^{18}O_2$ isotopic substitution experiments to be $Rh(O_2)_2$ and $Rh(O_2)$. The corresponding $^{16}O^{18}O$ infrared data spectroscopically indicate that the dioxygen moieties in both complexes are bonded to the rhodium atom in a dihapto (side-on) fashion. The UV–visible spectrum of $Rh(O_2)_2$ is recorded in O_2 matrices and is compared with that for the isostructural $Pd(O_2)_2$ complex. In an effort to understand the electronic structures of these interesting bis(dioxygen) complexes and the origin of the shifts in their UV absorptions, extended Hückel molecular orbital calculations are undertaken. An argument which favors a bis-superoxide formulation and an $O_2 \rightarrow M$ charge-transfer assignment for the observed UV bands of $Rh(O_2)_2$ and $Pd(O_2)_2$ is presented.

Introduction

The cryochemically controlled manipulation of metal atom reactions with themselves and with other molecules has pointed the way to a fundamental new method of examining small, well-defined "naked" metal clusters and "localized bonding" aspects of surface molecular states.[1] In particular, our recent thrust toward modeling catalytic intermediates on atomic, diatomic, and higher order metal cluster sites and relating the data to the chemisorbed state is beginning to yield intriguing new information about metal–ligand (pseudo-adsorbate–ad-

sorbent) interactions at the atomic and molecular levels which would normally be inaccessible by conventional chemical procedures.[1a-c] This novel approach to chemisorption and catalysis-related problems is significant in that it holds the possibility of bridging the gap between concepts in homogeneous and heterogeneous systems by performing controlled reactions on precisely defined metal cluster systems varying from single-metal-atom to few-atom sites. In this particular study, which is the first part of a two-part investigation of rhodium atom and rhodium cluster chemistry, we will be initially concerned with the embryonic stages of Rh_n agglomeration reactions. This will be followed by a detailed study of the cryochemical reactions of Rh atoms with dioxygen. The cryochemical reactions of Rh_n agglomerates with dioxygen[2] will constitute part 2 of this investigation.

The main impetus for these studies, besides the intriguing chemistry, is the hope that the data will bear a logical relationship to a number of problems in the area of heterogeneous oxidation catalysis by the supported noble metals. Therefore, the present investigation is primarily concerned with an attempt to gain an insight into the nature of dioxygen chemisorption on highly dispersed rhodium catalysts by way of model reaction intermediates of the form $Rh_n(O_2)_m$. These "localized bonding" models of the dioxygen chemisorbed state are generated in cryochemically controlled reactions of Rh atoms with O_2 and O_2/inert gas matrices.

Because of the fairly large number of products formed in these reactions and the detailed spectroscopic analyses required to establish rhodium and oxygen stoichiometry, we have divided the oxygen study into two parts, part 1 (this study) being mainly concerned with the synthesis and characterization of mononuclears $Rh(O_2)_n$ and part 2 focusing on binuclears and trinuclears, $Rh_2(O_2)_m$ and $Rh_3(O_2)_p$, respectively.[2]

Experimental Section

Rhodium atoms were generated by directly heating a rhodium filament (0.010 in.) or by heating a tungsten rod around which either Rh sheet (0.005 in.), Rh foil (0.001 in.), or Rh wire (0.20 in.) had been wound. All Rh metal was supplied by A. D. McKay of New York. Research grade $^{16}O_2$ (99.999%) and Ar (99.999%) were supplied by Matheson. Isotopically enriched $^{18}O_2$ (95%) and statistically scrambled $^{16}O_2/^{16}O^{18}O/^{18}O_2$ were obtained from Miles Research Laboratory. Rhodium was evaporated as previously described[5] and metal deposition rates were monitored using a quartz crystal microbalance.[6] CsI plates for the infrared and NaCl plates for the UV–visible experiments were cooled to 6 K by an Air Products liquid-helium transfer system or to 10–12 K by an Air Products Displex closed-cycle helium refrigerator. Spectra were recorded on a Perkin-Elmer 180 for the infrared and either a Unicam SP 8000 or a Varian Techtron 635 for the UV–visible experiments.

Results and Discussion

Rhodium Atom–Inert Gas Experiments. The chemistry of rhodium vapor has been explored recently but only to a limited extent.[7,8] Nevertheless, the few studies that have been undertaken, mainly by matrix cryochemical techniques, have indicated the pronounced tendency of Rh atoms to form binuclear complexes. The property of matrix surface diffusion and aggregation of Rh atoms was first recognized in a series of Rh/N_2 cocondensation experiments by the identification of $Rh_2(N_2)_x$ complexes (where x is probably 8).[7] Clearer evidence of the clustering processes involved was derived from quantitative Rh atom concentration experiments in CO matrices where both $Rh(CO)_4$ and $Rh_2(CO)_8$ were generated and characterized.[8] In the latter study both the statistical pathway to binuclear complex formation and the kinetics of the surface diffusion processes occurring in the reaction zone were analyzed and led, in both cases, to a simple expression for the ratio of the absorbances of binuclears (D) to mononuclears (M) of the form

$$A_D/A_M = K[M]_0$$

where $[M]_0$ is the total concentration of metal in the matrix reaction and K is a constant. This expression was shown to be valid up to metal/matrix ratios of about 1/100 to 1/20. It was realized at the time that this novel analytical technique for treating the absorbances of spectral lines in metal atom cryochemical experiments opened up a new and highly controlled way of probing the clustering processes of metal atoms with themselves to produce small, well-defined metal agglomerates[9] as well as with other molecules to form cluster complexes.[10] Since then a number of transition-metal diatomic molecules exemplified by Sc_2,[11] Ti_2,[11] V_2,[12] Cr_2,[9] Mn_2,[13a] Fe_2,[13a] Ni_2,[13b,c] Cu_2,[14] Nb_2,[15] Mo_2,[15] and Ag_2,[14] and bimetallics CrMo[29] as well as higher clusters Cr_3,[30] Mo_3,[30] Ni_3,[13c] Ag_3,[31] Ag_4,[31] Ag_5,[31] Ag_6,[31] Cr_2Mo,[30] and $CrMo_2$[30] have been generated and identified in low-temperature matrices, usually by quantitative UV–visible spectroscopy. In view of the $Rh_2(CO)_8$[8] and $Rh_2(N_2)_x$[7] results it was clearly important to establish the fate of Rh atoms when cocondensed with inert gas matrices in an effort to try to identify Rh_2 and possibly higher Rh_n clusters.

Additional incentives for seeking new experimental routes to small rhodium clusters of known composition relate to the well-known fact that supported rhodium (and iridium) catalysts are used industrially for a wide variety of hydrocarbon oxidation reactions.[3] Heterogeneous olefin oxidations in particular are perplexing in that a variety of partial oxidation products, ranging from aldehydes and acids to ketones and epoxides, can be formed depending on the choice of metal, support, dispersion, and reaction conditions.[3] For example, highly dispersed Rh/SiO_2 catalysts oxidize propylene mainly to acrolein[4] whereas Ir/SiO_2 yield mainly acetaldehyde.[3] In most cases, however, critical issues relating to the nature of the active sites and surface species, reaction mechanism, oxygen binding, structure sensitivity, and catalyst selectivity remain to be settled (see part 2 for further discussion of these points).

Besides the gas-phase absorption spectrum of atomic Rh,[16] only a single brief report, by Weltner et al.,[17] of matrix-isolated Rh atoms in Ne exists in the literature. As a result of the present study we shall demonstrate that a number of the spectral features attributed by Weltner et al.[17] to Rh atoms are in actual fact associated with Rh_2 molecules. Let us now formalize the spectral data.

When Rh atoms were cocondensed with Ar at high dilutions ($Rh/Ar \simeq 1/10^4$) the optical spectrum shown in Figure 1 was obtained. Table I lists the observed frequencies together with the corresponding gas-phase absorptions for a $^4F_{9/2}$ ground state.[16] Noteworthy is the blue shift of the order of 1000–5000 cm^{-1} for the absorptions of the isolated atom compared with those for the atom in the gas phase. The frequency shifts $\Delta\nu = \nu_g - \nu_m$ for the observed atomic lines of Rh in Ar relative to the respective gas-phase frequencies ν_g are displayed graphically in Figure 2 and show values not unlike those observed previously for other matrix-isolated metal atoms.[18]

When the rate of Rh atom deposition is increased at constant gas-deposition rate, retaining the total Rh metal concentration constant in each run, the absorptions associated with atomic Rh decrease (Table I) while absorptions at 344 and 325 nm and a group of at least two lines around 312 and 317 nm begin to grow in. Although the region around 315 nm is complicated because of band overlap with Rh atomic absorptions, the growth behavior of the new absorption at 344 nm relative to a well-defined Rh atom line (e.g., 276 nm) is quite clear. The spectra under high Rh concentration conditions (Figure 3) are quite striking, being dominated by the group of absorptions at 312/317 nm (coincident with those reported by Weltner et al.[17] to be Rh atoms). Under these

Table I. UV-Visible Absorption Spectra of Rh Atoms ($4d^8 5s^1$, $^4F_{9/2}$) Isolated in Ar, Kr, and Xe Matrices, Compared to the Gas Phase (cm^{-1})

ν_g	ν_M^{Ar}	$(\nu_m - \nu_g)^{Ar}$	ν_m^{Kr}	$(\nu_m - \nu_g)^{Kr}$	ν_m^{Xe}	$(\nu_m - \nu_g)^{Xe}$	Tentative designation
43 042	48 077	5035	46 948	3906	44643	1601	*a*
42 495							*a*
42 325	45 045	2720	43 668	1343	42918	593	*a*
41 953	43 103	1150	40 984	−969	40486	−1467	*a*
36 787	40 323	3536	36 900	113	36630	−157	$^4D_{7/2}$
32 004	36 242	4238	34 965	2961	34247	2243	$^2F_{7/2}$ or
31 102	36 242	5140	34 965	3863	34247	3145	$^4G_{7/2}$
29 431		4239	33 557	4126	33333	3902	$^4F_{9/2}$
	33 670						
29 105		4565	32 573	3468	32468	3363	$^4G_{11/2}$
28 543	32 051	3508	31 250	2707		2038	$^4G_{9/2}$
					30581		
27 075	31 546	4471	30 675	3600		3506	$^4D_{7/2}$

[a] State designation unknown.

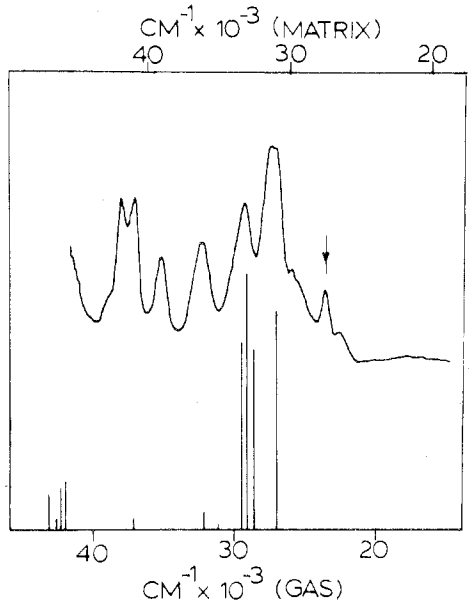

Figure 1. UV–visible spectrum of atomic Rh isolated in solid Ar at 10 K at high dilutions (Rh/Ar ≃ 1/10⁴) compared to gas-phase atomic transitions of Rh (stick heights correspond roughly to reported oscillator strengths).[16] The arrow depicts a Rh_2 absorption.

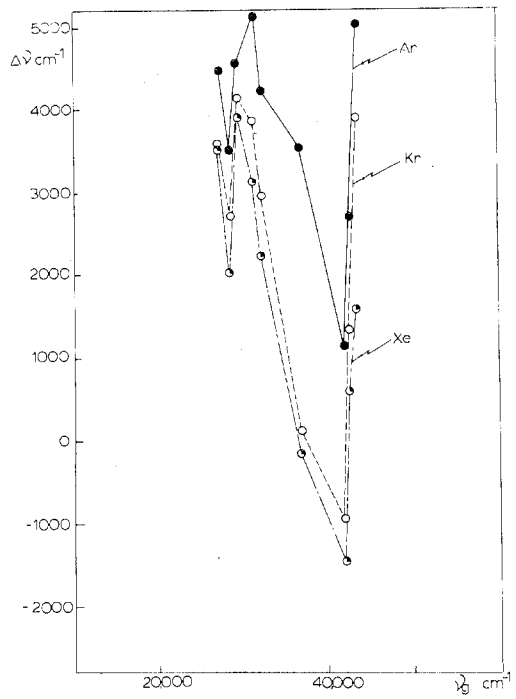

Figure 2. Graphical representation of the frequency shifts $\Delta\nu = \nu_g - \nu_m$ for the observed atomic lines of Rh in Ar, Kr, and Xe matrices, relative to the respective gas-phase frequencies ν_g.

conditions it is quite evident that band overlap occurs in the region 312/317 nm and makes quantitative appraisal of this group of lines difficult. However, the absorbance of the 344-nm band relative to that of a reference Rh atom band as a function of the Rh metal concentration shows a linear relationship and the corresponding log–log plot (Figure 4) shows a slope of 0.75, acceptably close to the theoretical value of unity predicted for Rh_2 generation. This serves to identify the absorption at 344 nm as an electronic transition of molecular Rh_2. (Note that at Rh/Ar ratios higher than those shown in Figure 3A, the group of absorptions at 312/317 and 325 nm shows identical intensity behavior to the absorption at 344 nm, indicating that they can all be associated with Rh_2.)

At this point it is important to inquire into the origin of the discrepancy between Weltner et al.[17] data and those of the present study.

As a part of Weltner's study of the ESR and UV–visible spectra of monomeric RhC,[17] the UV spectra of Rh atoms in Ne matrices were also investigated. His experiments involved the vaporization of Rh metal from an induction-heated tungsten cell with subsequent trapping in Ne matrices at about 4 K The reported Rh/Ne ratio was about 1/1000 although in situ crystal monitoring[6] similar to that of the present study was not employed. At first glance, the UV absorptions observed by Weltner et al.[17] appear to be similar to those reported in this study for atomic Rh in Ar matrices at 10–12 K.

Table II. Ultraviolet Spectra of Rh Vapor Cocondensed with Ne and Ar Matrices

Weltner et al.[17] "Rh" in Ne at 4.2 K, nm	Ozin et al. Rh in Ar at 10–12 K, nm	This study Rh_2 in Ar at 10–12 K, nm	Assignment
353.9	352		Rh
348.8		344	Rh_2
333.5	331		Rh
327.1	325[a]	325[a]	Rh + Rh_2
321.7	317[a]	317[a]	Rh + Rh_2
316.8	312[a]	312[a]	Rh + Rh_2
307.9	*b*		Rh
b	297		Rh
b	276		Rh
248.1	248		Rh
229.5	232		Rh
b	222		Rh
b	208		Rh

[a] Rh_3 or higher Rh_n aggregates could also contribute to the absorbances in this overlap region. [b] Not observed.

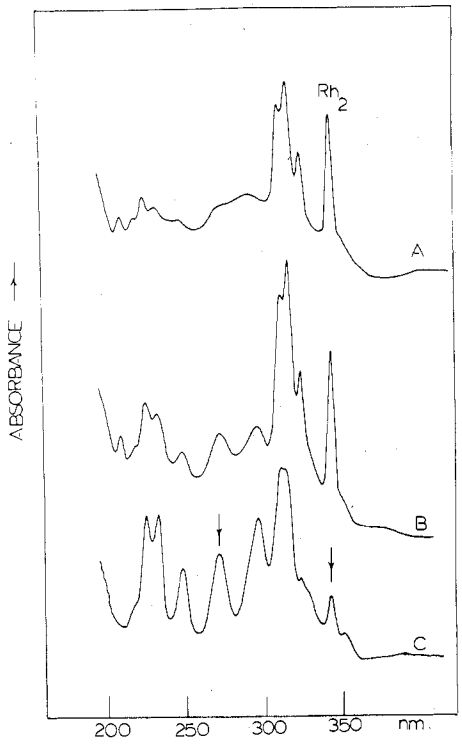

Figure 3. The UV–visible spectrum of atomic Rh isolated in solid Ar at 10 K showing the effect of increasing the Rh/Ar ratio (C to A) from roughly $1/10^4$ to $1/10^3$.

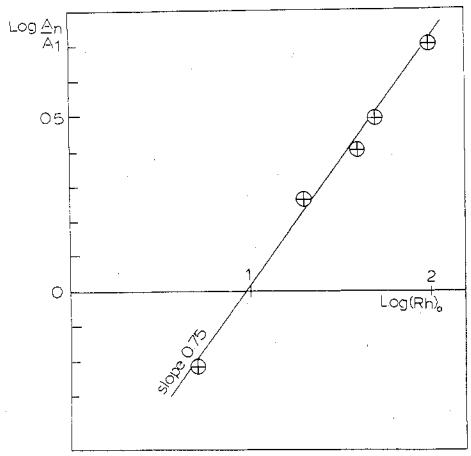

Figure 4. A log–log plot of the ratio of the absorbance of a line attributed to Rh_2 to that of a Rh atomic resonance absorption as a function of the rhodium metal depositiion rate at constant argon deposition rate.

However, closer examination (Table II) reveals the notable absence of strong Rh atomic lines observed by us in the region of 276 and 297 nm. The quantitative Rh concentration experiments of the present study show clearly that Rh atoms dimerize readily in Ar at ratios of $1/10^4$ to $1/10^3$ at 10–12 K. This effect is expected to be even more pronounced[9-14,18] in the more mobile matrix Ne even at 4.2 K. Thus it is not surprising that some of the absorptions assigned to Rh_2 in the present study correspond closely with those postulated by Weltner et al.[17] to be Rh atoms (Table II).

Weltner et al. realized at the time that a direct correlation of their supposed Rh atomic transitions in Ne matrices with those of the gas-phase compilation of Moore[16] for Rh atoms resulted in inconsistent matrix to gas-phase frequency shifts. Weltner et al. attempted to reconcile these discrepancies by resorting to multiple site effect and band overlap arguments for their Rh/Ne matrices.

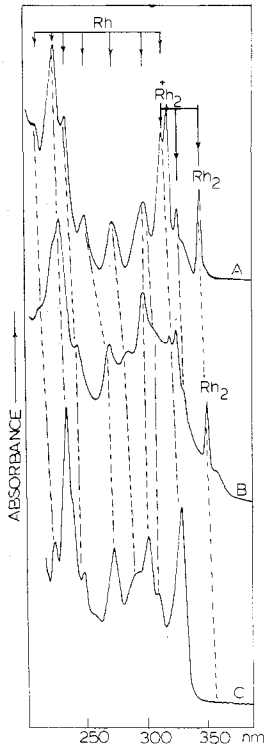

Figure 5. Correlation of the UV–visible spectrum of Rh atoms and Rh_2 molecules (A) in Ar, (B) in Kr, and (C) in Xe matrices under identical conditions of temperature, Rh metal deposition rate, and inert gas deposition rate.

We believe, on the basis of the Rh concentration experiments of the present study, that Weltner et al. had unknowingly generated large amounts of rhodium dimers and mistakenly assigned them to Rh atoms. This unfortunate error is now understandable in terms of the combined effects of the facile matrix surface diffusion and aggregation properties of Rh atoms coupled with a number of close coincidences between the UV absorptions of atomic Rh and molecular Rh_2, particularly in the region 345–310 nm (Table II).

Additional evidence for our spectral assignments of Rh atom absorptions stems from experiments in the more rigid matrices Kr and Xe. Considerable evidence now exists which supports the contention that, under identical conditions of metal and matrix deposition rates and deposition temperature, the more highly polarizable and rigid matrix Xe (and to a slightly lesser extent Kr) has a slightly higher quenching efficiency for isolating metal atoms under circumstances that favor dimers and higher clusters in Ne and Ar.[9-15] The results for Rh atoms in Xe and Kr shown in Figure 5, recorded under identical conditions to those in Ar shown in Figure 3, bear out this proposal. Correlation of the Rh atomic transitions on passing from Ar to Kr to Xe is relatively straightforward (Figure 5) and generally they display a red shift (Table I) for most of the observed lines, following the usual trend.[18] Particularly noteworthy is the absence of spectral lines around 350 nm in Xe, indicating that Rh_2 formation under these circumstances is indeed matrix impeded. Moreover, the simplicity of the 350–310-nm region for Xe matrices bears out our Rh/Rh_2 band overlap arguments described earlier for Ar matrices and apparent in Figure 5 for Kr matrices.

In concluding this first section we can state that the absorption spectra of Rh atoms isolated under high-dilution conditions in Ar, Kr, and Xe matrices have been observed and satisfactorily correlated with the known gas-phase UV transitions of atomic Rh. By studying these spectra as a function of the Rh deposition rate, retaining the total concentration of Rh metal constant, new spectral features have

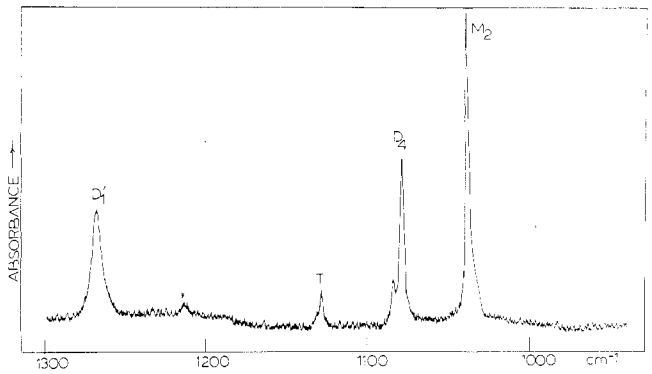

Figure 6. Matrix infrared spectrum of the products formed when Rh atoms are cocondensed with $^{16}O_2$ at 10–12 K and $Rh/^{16}O_2 \simeq 1/10^4$.

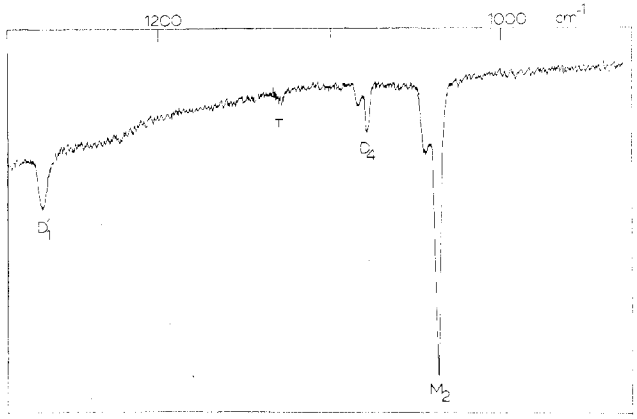

Figure 7. Same as Figure 6 except $Rh/^{16}O_2 \simeq 1/10^5$ was used.

been detected with growth characteristics of molecular Rh_2. Band overlap complications, however, rendered difficult the identification of Rh_3 and higher Rh_n clusters which are suspected also to be present in these matrices (see part 2 of this study[2]). The results of this investigation reinforce the idea that the lighter inert gases Ne and Ar isolate atomic species less efficiently than their heavier congeners Kr and Xe, so much so that spectra previously ascribed to Rh atoms isolated in Ne matrices are shown to belong predominantly to molecular Rh_2. The pronounced tendency of Rh atoms to dimerize at concentrations well below the statistical limit for appreciable Rh_2 formation indicates a very low activation energy for Rh–Rh bond formation at least for the dimer. This may be a consequence of the $4d^85s^1$ ($^4F_{9/2}$) electronic ground state being ideally set up for 5s–5s overlap, which by comparison with other transition metal diatomic molecules[19] is presumably the major orbital interaction contributing to the metal–metal bond. This facile dimerization property of Rh atoms to Rh_2 is certainly consistent with our earlier observation of $Rh_2(CO)_8$ formation in CO matrices.[8] In part 2 of this study,[2] we have taken advantage of the controlled aggregation reactions of Rh atoms to generate and study binuclear $Rh_2(O_2)_n$ and trinuclear $Rh_3(O_2)_m$ complexes in O_2 matrices. In what follows we describe our experiments with Rh atoms and dioxygen which lead to the new mononuclear complexes $Rh(O_2)_{1,2}$.

Rhodium Atom–Dioxygen Experiments. Preliminary matrix infrared experiments in which Rh atoms were cocondensed with pure $^{16}O_2$ matrices at 10–12 K, using a range of $Rh/^{16}O_2$ ratios, immediately indicated that one was dealing with a more complicated system than that previously encountered with the nearest neighbor atom, palladium.[20] The situation for the corresponding $Pd/^{16}O_2$ reactions under comparable conditions is quite simple, showing a single ν(OO) stretching frequency at 1112 cm^{-1} corresponding to a single product, $Pd(O_2)_2$.[20] A pseudotetrahedral D_{2d} structure containing side-on bonded dioxygen has been assigned to this complex[20] although the distinction between side-on and end-on bonded dioxygen, from $^{16}O_2/^{16}O^{18}O/^{18}O_2$ infrared isotopic studies, has been shown to be a difficult one.[21a]

The complexity of the $Rh/^{16}O_2$ system is best illustrated by reference to Figure 6 which shows the infrared spectrum in the ν(OO) stretching region on cocondensing Rh atoms with $^{16}O_2$ using a matrix ratio of roughly $1/10^4$. Unlike the corresponding $Pd/^{16}O_2$ reaction which displays a single absorption at 1112 cm^{-1}, the $Rh/^{16}O_2$ reaction shows at least *four* absorptions at 1265, 1130, 1078, and 1038 cm^{-1}, the relative intensities of which are found to be highly dependent on the $Rh/^{16}O_2$ ratio. A particularly fascinating feature of this spectrum is the extremely high ν(OO) stretching mode (1265 cm^{-1}), an unprecedented observation for coordinated O_2 in transition-metal dioxygen complexes.[22]

A further indication of the fruitful abundance of rhodium–dioxygen interactions stems from preliminary experiments in dilute $^{16}O_2/Ar \simeq 1/50$ mixtures. Whereas in the corresponding $Pd/^{16}O_2/Ar$ reaction one observes just two absorptions at 1111 and 1024 cm^{-1} associated with $Pd(O_2)_2$ and $Pd(O_2)$, respectively,[20] the $Rh/^{16}O_2/Ar$ experiment reveals at least *four* new absorptions at 922, 908, 904, and 890 cm^{-1} in addition to those observed in pure $^{16}O_2$ matrices.

From the results of our $Rh/Ar \simeq 1/10^4$ to $1/10^2$ experiments described earlier on in this study, which showed the coexistence of Rh atoms, Rh_2 molecules and possibly higher Rh_n clusters, it is apparent that the extension to O_2 and O_2/Ar matrices has opened the way to a number of $Rh_x(O_2)_y$ combinations. Therefore, in order to simplify the presentation of the experiments and spectroscopic analyses required to selectively synthesize and characterize the numerous $Rh_x(O_2)_y$ complexes in the Rh/O_2 system, we will devote the remainder of this paper exclusively to mononuclears while part 2 will concentrate on binuclears and trinuclears.[2] The discussion of the relevance of these data to the more complex, bulk chemisorption situation will also be reserved to part 2 of this study.[2]

Experiments Aimed at Identifying Mononuclear $Rh(O_2)_n$ Complexes. Infrared Experiments. In order to minimize surface diffusion and aggregation effects and promote Rh atom reactions and mononuclear complex formation, Rh atoms were cocondensed with pure $^{16}O_2$ at very high matrix dilutions, $Rh/^{16}O_2 \simeq 1/10^5$ at 10–12 K. A typical spectrum is shown in Figure 7 from which it can be seen that a ν(OO) absorption at 1038 cm^{-1} (M_2) dominates, followed in descending intensity order by weaker absorptions at 1265 (D_1'), 1078 (D_4), and 1130 (T) cm^{-1}. Weak, low-frequency absorptions, probably associated with Rh–O stretching motions,[20] were observed at 516, 480, and 440 cm^{-1}. On warming these matrices in the range 10–45 K, one observes the gradual decay of M_2, little change initially for D_4 and D_1', and slight growth for T. Continued warming causes D_1' to decay at a faster rate than D_4, while T remains roughly unchanged. Eventually T begins to decay. These data, coupled with Rh concentration experiments to be described later,[2] point to the coexistence of *four different* compounds in O_2 matrices designated M_2, D_4, D_1', and T. The species absorbing at 1038 cm^{-1} (M_2) would appear to be the *highest* stoichiometry mononuclear complex, namely $Rh(O_2)_n$. This can be ascertained from a combination of high- and low-concentration $^{16}O_2/Ar$ and $^{16}O_2/Xe$ experiments taken in conjunction with $^{16}O_2/^{18}O_2$ and $^{16}O_2/^{16}O^{18}O/^{18}O_2$ isotopic substitution experiments. To minimize surface diffusion and aggregation effects and thereby simplify the identification of mononuclear reaction products, the rigid matrix $^{16}O_2/Xe \simeq 1/25$ was chosen.

Under these conditions the major absorptions occur at 1045 (M_2) and 900 (M_1) cm^{-1}, with weak bands at 913 (D_1) and

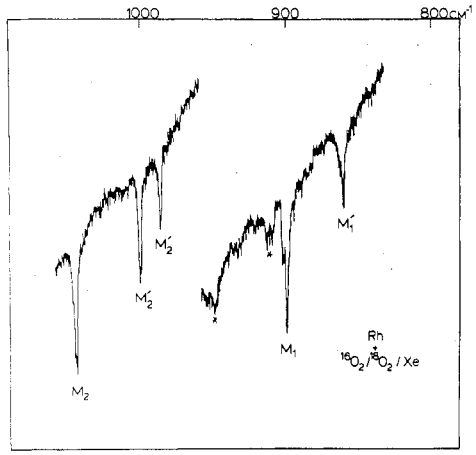

Figure 8. Matrix infrared spectrum of the products formed when Rh atoms are cocondensed with $^{16}O_2/^{18}O_2/Xe \simeq 2/1/50$ at 10–12 K, showing the isotope patterns of M_2, $Rh(^{16}O_2)_n(^{18}O_2)_{2-n}$, and M_1, $Rh(^{16}O_2)_m(^{18}O_2)_{1-m}$ (where $n = 0$–2 and $m = 0$–1). Asterisks indicate cluster and/or impurity lines—see Appendix and ref 2.

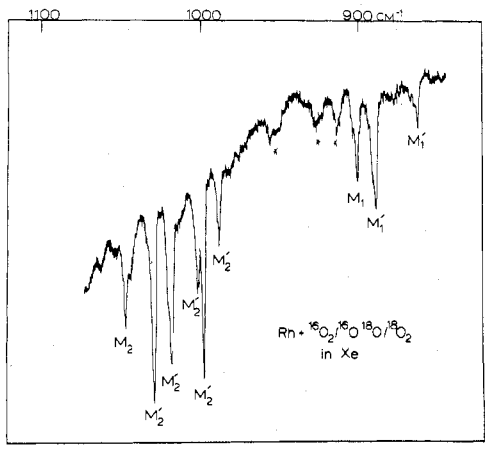

Figure 9. Same as Figure 8 except $^{16}O_2/^{16}O^{18}O/^{18}O_2/Xe \simeq 1/2/1/50$ mixtures were used, showing the isotope patterns of M_2, $Rh(^nO^mO)_2$, and M_1, $Rh(^nO^mO)$ (where $n, m = 16$ or 18). Asterisks indicate cluster and/or impurity lines—see Appendix and ref 2.

1072 (D_4) cm^{-1}. Warmup experiments performed on these matrices show the gradual decay of M_1 followed by M_2 at 30–40 K. Concomitant with this loss of the major absorbing species, one observes the growth of absorptions at 1123 (T), and 1072 (D_4), and 892 (D_3) cm^{-1}. Apart from small matrix-induced frequency shifts, it would appear that species M_2, D_4, and T are common to both $^{16}O_2$ and $^{16}O_2/Xe \simeq 1/25$ matrices. Moreover, the Xe results would tend to indicate that species M_1, absorbing at 900 cm^{-1} in Xe, is a mononuclear dioxygen complex with a *lower* stoichiometry than that of M_2, absorbing at 1045 cm^{-1} in Xe and 1038 cm^{-1} in $^{16}O_2$. Similar experiments in dilute $^{16}O_2/Ar \simeq 1/50$ to 1/250 mixtures place M_1 and M_2 at 908 and 1048 cm^{-1}, respectively, although the more pronounced aggregation properties of Rh atoms in Ar compared to Xe[9-12] resulted in other species in addition to M_1, M_2, D_4, D_3, and T being observed. These species turn out to be exclusively binuclear and higher clusters and are more pertinent to part 2 of this study.[2]

To establish the dioxygen stoichiometry in our proposed mononuclear complexes M_1 and M_2, we performed the corresponding $^{16}O_2/^{18}O_2/Xe \simeq 1/1/50$ and $^{16}O_2/^{16}O^{18}O/^{18}O_2/Xe \simeq 1/2/1/50$ experiments. A typical series of infrared data is displayed in Figures 8 and 9, from which it can be seen that the original absorption of M_2 at 1045 cm^{-1} in $^{16}O_2/Xe$ appears as a well-defined isotopic *triplet* in $^{16}O_2/^{18}O_2/Xe$ and an isotopic *sextet* in $^{16}O_2/^{16}O^{18}O/^{18}O_2/Xe$ matrices. Furthermore, the original absorption of M_1 at 900 cm^{-1} in $^{16}O_2/Xe$ appears as an isotopic *doublet* in $^{16}O_2/^{18}O_2/Xe$ and an isotopic *triplet* in $^{16}O_2/^{16}O^{18}O/^{18}O_2/Xe$ (see Tables III and IV for the list of isotopic frequencies). The corresponding isotopic structure observed in $^{16}O_2/^{18}O_2/Ar$ and $^{16}O_2/^{16}O^{18}O/^{18}O_2/Ar$ mixtures is listed in Table V.

At this point we recognize the fact that the isotopic frequency data for M_2 and M_1 show a striking resemblance to the corresponding data collected earlier for $Pd(O_2)_2$ and $Pd(O_2)$, respectively[20] (Table V) and point immediately to an analogous $Rh(O_2)_2$ and $Rh(O_2)$ formulation. Let us formalize our stoichiometric and structural assignments, beginning with M_2. The triplet pattern in $^{16}O_2/^{18}O_2/Xe$ mixtures indicates that the absorbing species contains *two* equivalent dioxygen molecules and the lines are easily assigned to the isotopic species $(^{16}O_2)Rh(^{16}O_2)$, $(^{16}O_2)Rh(^{18}O_2)$, and $(^{18}O_2)Rh(^{18}O_2)$ as shown in Table III. In principle, the mode of attachment of the dioxygen molecules to the metal in a bis(dioxygen) compound can be determined from $^{16}O^{18}O$ experiments, and indeed, with the scrambled $^{16}O_2/^{16}O^{18}O/^{18}O_2/Xe$ mixture, the original absorption at 1045 cm^{-1} in $^{16}O_2/Xe$ splits into a *six*-line spectrum which can be assigned to the possible isotopic combinations of a $(O_2)Rh(O_2)$ molecule as shown in Table

Table III. Observed and Calculated Infrared Isotopic Data for $Rh(^nO^mO)_2$ (Where $n, m = 16$ or 18)

Obsd freq[a] (Xe matrices)	Calcd freq[a,b]	Assignment
1045	1047	$Rh(^{16}O_2)_2$
1030	1028	$Rh(^{16}O_2)(^{16}O^{18}O)$
1018	1017	$Rh(^{16}O^{18}O)_2$
1001	1002	$Rh(^{18}O_2)(^{16}O_2)$
998	998	$Rh(^{18}O_2)(^{16}O^{18}O)$
987	987	$Rh(^{18}O_2)_2$

[a] Units in cm^{-1}. [b] Based on a Cotton-Kraihanzel frequency factored force field; $k_{OO} = 5.42$, $k_{OO,OO} = 0.25$ mdyn/A; cf. $Pd(O_2)_2$ which has $k_{OO} = 6.24$ and $k_{OO,OO} = 0.41$ mdyn/A.

Table IV. Observed and Calculated Frequencies and MVFF Force Constants for $M(^nO^mO)$ (Where M = Rh or Pd and $n, m = 16$ or 18)

$Rh(O_2)$[a]		$Pd(O_2)$[a]		
Obsd[c]	Calcd[e]	Obsd	Calcd	Assignment[b]
900	908	1024	1024	$M(^{16}O_2)$
888	884	996	995	$M(^{16}O^{18}O)$
862	859	967	966	$M(^{18}O_2)$
422	(425)[d]	427	427	
2.85		4.15		k_{OO}
1.84		1.35		k_{MO}
0.62		0.45		$k_{MO,OO}$
0.44		0.24		$k_{MO,MO}$

[a] Frequencies in cm^{-1}. [b] Force constants in mdyn/A. [c] Xe matrices. [d] Estimated value. [e] Potential energy distribution matrix indicates considerable mixing between the symmetric O-O and Rh-O stretching modes; that is 908 cm^{-1}, 18% ν(RhO), 82% ν(OO); and 425 cm^{-1}, 59% ν(RhO), 41% ν(OO).

Table V. Comparison of the Infrared Isotopic Data for $Rh(^nO^mO)_2$ and $Pd(^nO^mO)_2$[b]

M = Rh[a] (in Ar)	M = Pd[a] (in Ar)	Molecule
1048	1112	$M(^{16}O_2)_2$
1028	1092	$M(^{16}O_2)(^{16}O^{18}O)$
1018	1081	$M(^{16}O^{18}O)_2$
1003	1067	$M(^{16}O_2)(^{18}O_2)$
1000	1061	$M(^{18}O_2)(^{16}O^{18}O)$
987	1049	$M(^{18}O_2)_2$

[a] Frequencies in cm^{-1}. [b] $n, m = 16$ or 18.

III. This *sextet* pattern indicates a nondegenerate vibration of two equivalent dioxygen molecules, each containing equivalent oxygen atoms. The second and fifth components of the multiplet indicate the equivalence of the oxygen atoms in each O_2 unit, since, if the molecules were attached in an end-on fashion (nonequivalent), further splitting or line broadening of the lines due to the rearrangement of the ($^{16}O^{18}O$) component would be expected. This broadening is not obvious. The absence of the lines assigned to the species $Rh(^{16}O^{18}O)_2$ in $^{16}O_2/^{18}O_2$/Xe matrices and the nonequivalence of the (16–16)(18–18) and (16–18)(16–18) species indicated in the spectrum show that the original oxygen molecules remain *intact* upon bonding to the metal atom.

Since a planar (D_{2h}) structure would have cis and trans isomers for the (16–18)(16–18) molecule and since no obvious splitting is observed at the frequency assigned to the species (1018 cm^{-1}), the D_{2d} "spiro" structure is proposed for $Rh(O_2)_2$. By similar reasoning, the *doublet* pattern in $^{16}O_2/^{18}O_2$/Xe mixtures observed for species M_1 would indicate a mono(dioxygen) formulation, $Rh(O_2)$. The absence of a central component in this experiment also demonstrates that the original oxygen molecules remain intact upon bonding to the metal atom. The *triplet* pattern in $^{16}O_2/^{16}O^{18}O/^{18}O_2$/Xe mixtures (Table IV) confirms the $Rh(O_2)$ assignment and serves to identify the $Rh(^{16}O^{18}O)$ molecule. The absence of a discernible splitting on the $Rh(^{16}O^{18}O)$ absorption would tend to support side-on bonding of the dioxygen to the metal, *although caution must be exercised here (as well as with $Rh(O_2)_2$)*, as it is possible that for bandwidths of the order of 2–4 cm^{-1} one might not resolve a small splitting, indicative of end-on bonding.[21a] For the purpose of the discussions which follow, we will assume that a side-on coordination scheme is operative.[21b]

Bis(dioxygen)rhodium, $Rh(O_2)_2$. In view of the striking resemblance of the dioxygen isotope pattern of $Rh(O_2)_2$ to that of $Pd(O_2)_2$ and the success of the frequency factored force field approximation for reproducing the isotopic frequencies of $Pd(^nO^mO)_2$ (where n, m = 16 or 18),[20] we decided to perform a similar type of calculation for the respective $Rh(^nO^mO)_2$ molecules. The best fit frequencies and k_{OO}, $k_{OO,OO}$ force constants that result from this calculation are listed in Table III.

Mono(dioxygen)rhodium, $Rh(O_2)$. The asymmetric $^{16}O_2/^{16}O^{18}O/^{18}O_2$ isotopic triplet pattern observed for Rh($^nO^mO$) (where n, m = 16 or 18) shown in Figure 9 and Table IV is interesting in that it indicates a breakdown of the frequency factored force field approximation for this molecule. With the knowledge that the low-frequency ν(RhO) stretching mode of $Rh(O_2)_2$ occurs in the region 516–480 cm^{-1} and that $Pd(O_2)_2$ and $Pd(O_2)$ show corresponding ν(PdO) modes at 504 and 427 cm^{-1}, respectively,[20] we undertook a modified valence force field (MVFF) calculation for an isosceles C_{2v} triangular $Rh(O_2)$ molecule (similar to that described in ref 20), assuming that the ν(RhO) mode is somewhere in the range of 450–400 cm^{-1}. The dependence of the ν(OO) and ν(RhO) frequencies on the values of k_{OO}, k_{RhO} and suitable interaction force constants was thoroughly searched and resulted in the force field frequencies listed in Table IV. The reasonably close agreement between the observed and calculated frequencies for $Rh(O_2)$ provides evidence for appreciable metal–ligand vibrational coupling in the molecule, which is to be contrasted with the apparently weaker coupling effects in $Rh(O_2)_2$ as indicated by the results of the frequency factored force field calculations shown in Table III.

The corresponding force field for $Pd(^nO^mO)$ (where n, m = 16 or 18) is included in Table IV for the purpose of comparison. An interesting trend in the ν(OO) stretching frequencies and k_{OO} bond stretching force constants is noteworthy, $Pd(O_2) > Rh(O_2)$ and $Pd(O_2)_2 > Rh(O_2)_2$, and will be discussed later.

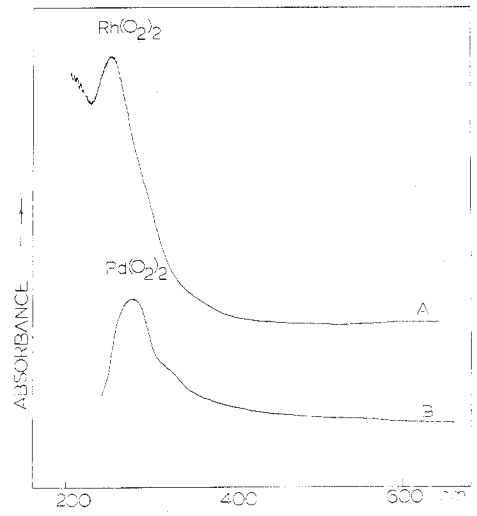

Figure 10. UV–visible spectrum of the products formed when (A) Rh atoms and (B) Pd atoms are cocondensed with $^{16}O_2$ at 10–12 K and $M/^{16}O_2 \simeq 1/10^5$.

UV–Visible Experiments. When Rh atoms are cocondensed with $^{16}O_2$ matrices under conditions which favor dominant amounts of $Rh(O_2)_2$, one observes an intense UV absorption around 250 nm (Figure 10A). For the purposes of comparison, we performed a similar experiment with Pd atoms to yield $Pd(O_2)_2$ for which a typical spectrum is shown in Figure 10B. Evidence for weak absorptions in the range 400–900 nm could not be found for either compound.

Electronic Properties of $Rh(O_2)_2$ and $Pd(O_2)_2$. Taken in isolation, the UV–visible spectrum of $Rh(O_2)_2$ is not terribly informative, as the only observable spectral feature is a strong absorption centered at roughly 250 nm. However, when it is taken in conjunction with the corresponding data for the isostructural complex $Pd(O_2)_2$ (Figure 10A, B), one can make a number of definitive statements. To begin, one can see that, apart from a weak shoulder at roughly 320 nm on the strong absorption at 280 nm for $Pd(O_2)_2$, the optical spectra of $Pd(O_2)_2$ and $Rh(O_2)_2$ are essentially identical. The main UV absorption of $Pd(O_2)_2$ (280 nm) is *red* shifted relative to the corresponding absorption of $Rh(O_2)_2$ (250 nm). However, neither complex shows evidence for absorption in the range 350–900 nm. By comparison with the optical data for O_2^- trapped in alkali halide crystals and alkaline earth superoxides $M^+O_2^-$ isolated in inert gas matrices[23] (which show the $\pi \rightarrow \pi^*$ type transition of superoxide in the region of 250 nm), one is initially tempted to assign the UV absorptions of $Rh(O_2)_2$ and $Pd(O_2)_2$ to a similar type of "localized" intraligand transition of coordinated superoxide in an $M^{2+}(O_2^-)_2$ complex. However, certain observations argue against this assignment. First, known paramagnetic rhodium(II) complexes such as $RhCl_2\{(o\text{-tol})_3P\}_2$ are blue-green in color,[24] whereas $Rh(O_2)_2$ in low-temperature O_2 matrices is essentially colorless. This fact alone would argue against a simple pseudotetrahedral bis(superoxo)rhodium(II) formulation for $Rh(O_2)_2$. Second, the infrared-active ν(OO) stretching mode and k_{OO} bond stretching force constants follow the order $Pd(O_2)_2 > Rh(O_2)_2$. This would imply a higher O–O bond order and a correspondingly greater ($\pi \rightarrow \pi^*$)-type transition energy for the $Pd(O_2)_2$ complex. This is the opposite trend to that observed in practice. Recalling that the valence orbital ionization potentials for the 4d, 5s, and 5p levels of atomic Pd are higher than those of Rh (see Table VI), one might further predict that metal-to-ligand charge-transfer transitions should follow the order $Pd(O_2)_2 > Rh(O_2)_2$. This is not the case in practice

Table VI. Parameters Used in the Extended Hückel Molecular Orbital Calculations for Pseudotetrahedral $(O_2)Rh(O_2)$ and $(O_2)Pd(O_2)$[a]

	Orbital	Orbital exponent	H_{ii},[b] eV
Rh	4d	3.491	−7.89
	5s	1.544	−7.32
Pd	4d	3.646	−8.52
	5s	1.584	−7.44
O	2s	2.246	−32.33
	2p	2.227	−15.80

[a] Bond lengths used in the calculations r(Rh–O) = 2.0 Å, r(O–O) = 1.40 Å, r(Pd–O) = 2.0 Å, and r(O–O) = 1.40 Å. [b] Cusachs approximation used (*J. Chem. Phys.*, 43, 5157, (1965)) with unmodified Baranovskii Coulomb integrals (*Teor. Eksp. Khim.*, 3, 527 (1967)) and Clementi–Roetti orbital exponents ("Atomic and Nuclear Data Tables", Vol. 14, Academic Press, New York, N.Y., 1974, p 445).

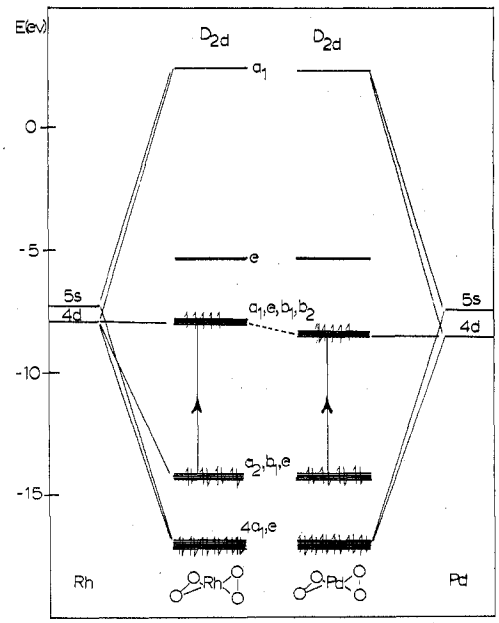

Figure 11. Extended Hückel molecular orbital energy level schemes calculated for pseudotetrahedral $(O_2)M(O_2)$, where M = Rh or Pd (see text for notation and Table VI for the parameters used in the calculations).

and could be an argument against an $M \rightarrow O_2$ charge-transfer assignment for the observed UV absorptions. Contrariwise, an $O_2 \rightarrow M$ charge-transfer assignment would be expected to follow the observed spectral trend, $Rh(O_2)_2 > Pd(O_2)_2$.

In an attempt to gain an insight into the credibility of this spectral assignment, we decided to investigate the electronic structures of $Rh(O_2)_2$ and $Pd(O_2)_2$ by extended Hückel molecular orbital techniques. In these calculations the 4d and 5s orbitals of atomic Rh and Pd were employed together with Clementi–Roetti orbital exponents, the Cusach approximation, and unmodified Baranovskii values for the Coulomb integrals (Table VI). For an assumed D_{2d} pseudotetrahedral geometry and the parameters listed in Table VI, we obtained the energy level scheme for $Rh(O_2)_2$ and $Pd(O_2)_2$ as shown in Figure 11. The general molecular orbital picture that emerges for $Rh(O_2)_2$ and $Pd(O_2)_2$ (although somewhat unrealistic) is one that substantiates an $O_2 \rightarrow M$ charge-transfer assignment for the observed UV spectral absorptions. In essence we find that a group of six orbitals centered around −17 eV have considerable σ and π dioxygen character. Two of this group contribute to the metal–dioxygen σ-bonding interaction. The next highest collection of orbitals centered around −14 eV are best described as dioxygen π^*-type orbital combinations. The lowest degenerate level of these has a small $M(d\pi) + O_2(\pi^*)$ bonding contribution. Finally in the region around −8 eV, a group of partially filled, closely spaced, metal d orbitals occur (note that d-orbital splittings are usually highly underestimated by extended Hückel techniques[29]).

With this qualitative energy level scheme it would appear that the intense UV transition at 250 nm for $Rh(O_2)_2$ originates in charge transfer between the dioxygen π^* levels around −14 eV and the appropriate d level(s) around −8 eV. On passing to $Pd(O_2)_2$ the dioxygen π^* levels remain essentially unperturbed (Figure 11) whereas the metal d levels are stabilized by about 4300 cm^{-1}. On these grounds we expect a red shift of roughly 4300 cm^{-1} in the UV $O_2 \rightarrow M$ charge-transfer transition which is fortuitously close to the observed red shift of roughly 5000 cm^{-1} (Figure 10).

In an attempt to check on the sensitivity of the molecular orbital energy-level ordering and total energy of $Rh(O_2)_2$, with respect to variations in molecular geometry, we computed

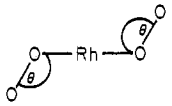

i

as a function of θ for the all-planar structure

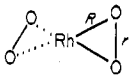

ii

as a function of r and R and

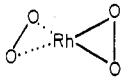

iii

in the D_{2d}, D_{2h}, and D_2 configurations.

In brief, we find that within the framework of extended Hückel theory, the effect of changing the geometry of $Rh(O_2)_2$ from D_{2d} to D_{2h} to D_2 (retaining side-on bonded dioxygen with r(O–O) = 1.4 Å and r(Rh–O) = 2.0 Å) has a minimal effect on the total energy (0.02 eV was the maximum computed energy difference between the three forms) as well as the overall form of the molecular orbital energy level scheme. On retaining the r(Rh–O) bond length constant at 2.0 Å one finds a trend to greater stability as the r(O–O) bond length is varied from 1.3 to 1.6 Å although a minimum was not encountered at the 1.6-Å extreme. Similar calculations, in which the r(O–O) bond distance was held constant at 1.4 Å, indicated a trend to greater stability as the r(Rh–O) bond distance decreased from 2.1 to 1.9 Å, although once again an energy minimum was not reached at the 1.9-Å extreme used in these calculations. Finally, we computed the total energy of $Rh(O_2)_2$ as a function of side-on vs. end-on bonded dioxygen by varying the angle θ shown in (i) above, retaining the r(Rh–O) = 2.0 Å and r(O–O) = 1.4 Å. Interestingly, the side-on geometry for the coordinated dioxygen moiety appears to be favored in these calculations for $Rh(O_2)_2$ (perhaps fortuitously in line with our $^{16}O_2/^{16}O^{18}O/^{18}O_2$ infrared isotopic data) with an energy minimum corresponding to θ in the range of 60°.

Although these calculations quantitatively reveal the gross features of the electronic structure of $M(O_2)_2$ (M = Rh, Pd) we fully realize that the energy level and bonding picture that emerges is not particularly realistic. As is commonly found with EHMO calculations for transition-metal systems, the d-orbital splittings are severely underestimated[29] and as a result the exact designation of the levels involved in LMCT is essentially impossible. In fact, for this set of circumstances, simple molecular orbital based symmetry arguments, taking

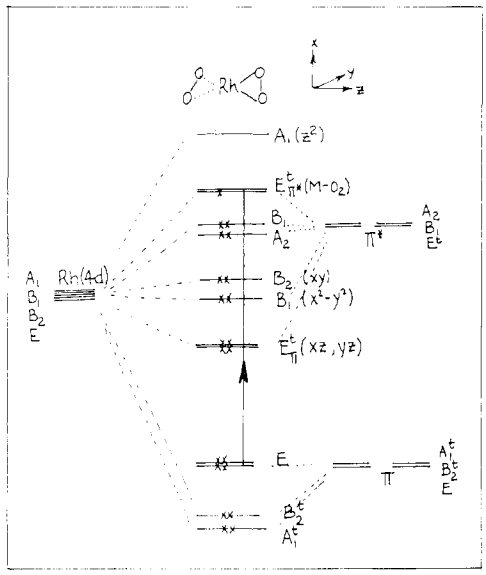

Figure 12. Symmetry-based molecular orbital energy level scheme for pseudotetrahedral $(O_2)Rh(O_2)$, illustrating the proposed UV LMCT transition (see text) and its relationship to an "intraligand" $\pi \rightarrow \pi^*$ type of transition.

into account Rh(d)–$O_2(\pi/\pi^*)$ orbital mixing, are somewhat more informative.

To illustrate this point, consider pseudotetrahedral $M(O_2)_2$ with the Cartesian axes shown below

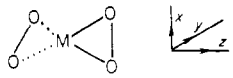

Concentrating on the dioxygen pπ orbitals, one can derive a symmetry classification in terms of those π orbitals pointing toward M, namely

$$\Gamma_{p\pi} = A_1^t + B_2^t + E^t$$

and those pointing perpendicular to the above, namely

$$\Gamma_{p\pi} = A_2 + B_1 + E$$

(The dioxygen π orbitals in $M(O_2)_2$ span the representation $A_1^t + B_2^t + E$, whereas dioxygen π^* span $A_2 + B_1 + E^t$; superscript "t" denotes an orbital spacially directed *toward* the central metal atom.) Assuming that the dioxygen π/π^* levels in $M(O_2)_2$ roughly straddle the 4d levels of Rh and Pd (which is not unreasonable for coordinated $O_2^{\delta-}$ in $M(O_2)_2$, where $1 \leq \delta \leq 2$) then one can construct the energy level scheme shown in Figure 12 for $M(O_2)_2$. In this formulation of the electronic structure of D_{2d} $(O_2)M(O_2)$ one obtains two low lying M–O_2 σ-type bonding orbitals ($A_1^t + B_2^t$) and an approximately nonbonding $O_2^{\delta-}$, E(π) level at somewhat higher energies. For the metal d orbitals, one would probably not argue that the M–O_2 $E_\pi^t(d_{xz}, d_{yz})$ experiences the greatest degree of π stabilization followed by the $B_1(x^2 - y^2)$. However, the exact ordering of the upper $B_2(xy)$, $A_2 + B_1(O_2^{\delta-}, \pi^*$ nonbonding), $E_{\pi^*}^t$(M–O_2), and $A_1(z^2)$ levels is not immediately obvious and will critically depend on the extent of charge transfer from the metal to the dioxygen ligands. This key question is illustrated in Figure 13 where it can be seen that at least four reasonable energy level schemes can be constructed for the upper five levels (M becoming increasingly positive on passing from left to right in Figure 13, say $M^0(O_2^0)_2$ to $M^{II}(O_2^{-I})_2$). Clearly this electronic description of $M(O_2)_2$ predicts a number of *low-energy* LMCT and MLCT transitions. We do not observe any of these, presumably because they lie beyond the low-energy range of our UV–visible spectrometer, 200–900 nm. However, a feature of Figure 12 that is reasonably clear concerns an allowed transition from

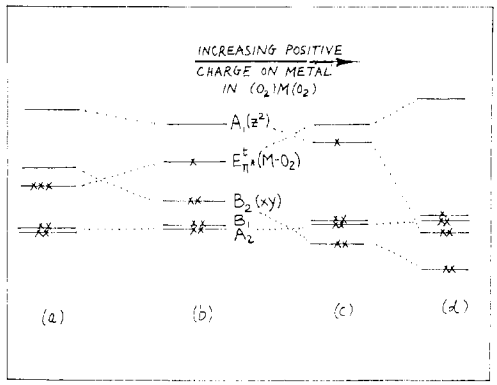

Figure 13. Qualitative dependence of the upper five levels of $(O_2)Rh(O_2)$ (Figure 12) on the charge on the central rhodium atom (becoming increasingly positive on passing from (a) to (d)).

the low-lying E(π-O_2) nonbonding type levels to a vacancy in the upper $E_{\pi^*}^t$(M–O_2) levels which should *red* shift on passing from Rh to Pd. Actually, Figure 13 can be used to illustrate this point, as the effect of increasing the positive charge on the Rh is similar to that on passing from Rh to Pd (where the 4d levels are stabilized by about 0.5 eV). In a sense, the E(π-O_2) $\rightarrow$ $E_{\pi^*}^t$(M–O_2) transition can be described as LMCT but with a close resemblance to an $O_2^{\delta-}$ "intraligand" $\pi \rightarrow \pi^*$ type of transition (expected in the 250–300-nm region). The exact description of the levels giving rise to this UV band depends of course on the extent of $M(4d_{xz,yz})$–$O_2(\pi^*)$ orbital mixing. Considerable effort will be needed to clarify this interesting point.[21b]

Acknowledgment. This research was completed while G.A.O. was a Sherman-Fairchild Distinguished Scholar (1977) at Caltech. The hospitality of the Chemistry Division of California Institute of Technology is gratefully appreciated. Discussions with Professors W. A. Goddard III, H. B. Gray, and A. B. P. Lever, concerning the electronic spectroscopy, proved to be most helpful. We gratefully acknowledge the financial assistance of the National Research Council of Canada, the Atkinson Foundation, the Connaught Fund, Imperial Oil of Canada, the Lash Miller Chemistry Laboratories, and Erindale College. An NRCC Scholarship awarded to A.J.L.H. is also gratefully appreciated.

Appendix

Impurity Lines and Doping Experiments Throughout most of the Rh/O_2, $Rh/O_2/Ar$, and $Rh/O_2/Xe$ experiments performed in this study, *three* absorptions were observed in the regions 1220/1210, 1020/1010, and 960/950 cm^{-1} which displayed irreproducible intensity behavior between similar runs. Knowing that trace amounts of CO_2 and N_2 impurities[28] can cause parasitic absorptions to appear in metal atom matrix experiments,[25] we undertook a number of doping experiments in this study in order to establish the origin of these so-called "irreproducible" lines.

To begin with, $N_2/O_2/Ar$ doping experiments indicated that, besides the generation of the known compounds $Rh(N_2)_{1-4}$,[26] at least two other compounds could be formed with ν(NN) absorptions in the region of 2253 and 2280 cm^{-1}. Under these conditions the suspect bands at 1020/960 cm^{-1} appeared surprisingly intense relative to the $Rh_x(O_2)_y$ bands (together with a new 940-cm^{-1} band), indicating that they be assigned with the 2253/2280-cm^{-1} bands to $Rh(N_2)_n(O_2)_m$ complexes similar to the recently characterized $Pd(N_2)_n(O_2)$ complexes.[27]

Similar $CO_2/O_2/Ar$ doping experiments showed the anomalously high growth of an absorption around 1220 cm^{-1}, indicating that the suspect band in this region is most probably some kind of $Rh(O_2)_n(CO_2)_m$ complex.

Therefore in the spectral analyses of the $Rh_x(O_2)_y$ complexes these "impurity lines" were not considered.

Registry No. $Rh(^{16}O_2)_2$, 63904-17-6; $Rh(^{16}O_2)(^{16}O^{18}O)$, 63884-20-8; $Rh(^{16}O^{18}O)_2$, 63884-19-5; $Rh(^{18}O_2)(^{16}O_2)$, 63866-48-8; $Rh(^{18}O_2)(^{16}O^{18}O)$, 63884-18-4; $Rh(^{18}O_2)_2$, 63866-47-7; $Rh(^{16}O_2)$, 63884-17-3; $Rh(^{16}O^{18}O)$, 63884-16-2; $Rh(^{18}O_2)$, 63848-54-4; Rh, 7440-16-6; Rh_2, 12596-98-4; $Pd(O_2)_2$, 63848-53-3.

References and Notes

(1) (a) G. A. Ozin, *Acc. Chem. Res.*, **10**, 21 (1977); *Catal. Rev.*, in press; (b) H. Huber, G. A. Ozin, and W. J. Power, *J. Am. Chem. Soc.*, **98**, 6508 (1976); W. J. Power and G. A. Ozin, *Inorg. Chem.*, **16**, 212 (1977); (c) D. McIntosh and G. A. Ozin, *Inorg. Chem.*, 16, 59 (1977); H. Huber and G. A. Ozin, *ibid.*, **16**, 64 (1977); (d) R. Ugo, *Catal. Rev.*, **11**, 225 (1975); E. L. Muetterties, *Bull. Soc. Chim. Belg.*, **84**, 959 (1975); K. H. Johnson and R. P. Messmer, *J. Vac. Sci. Technol.*, **11**, 236 (1975), and references therein.

(2) A. J. L. Hanlan and G. A. Ozin, *Inorg. Chem.*, following paper in this issue.

(3) See for example N. W. Cant and W. K. Hall, *J. Catal.*, **16**, 220 (1970); **27**, 70 (1972), and references therein.

(4) N. W. Cant and W. K. Hall, *J. Catal.*, **23**, 287, (1971); *J. Phys. Chem.*, **75**, 2914 (1971), and references therein.

(5) E. P. Kündig, M. Moskovits, and G. A. Ozin, *J. Mol. Struct.*, **14**, 137 (1972).

(6) M. Moskovits and G. A. Ozin, *J. Appl. Spectrosc.*, **26**, 487 (1972).

(7) G. A. Ozin and A. Vander Voet, *Can. J. Chem.*, **51**, 3332 (1973).

(8) L. A. Hanlan and G. A. Ozin, *J. Am. Chem. Soc.*, **96**, 6324 (1974).

(9) E. P. Kündig, M. Moskovits, and G. A. Ozin, *Nature (London)*, **254**, 503 (1975).

(10) H. Huber, E. P. Kündig, G. A. Ozin, and A. J. Poe, *J. Am. Chem. Soc.*, **97**, 308 (1975); H. Huber, E. P. Kündig, M. Moskovits, and G. A. Ozin, *ibid.*, **97**, 2097 (1975); E. P. Kündig, M. Moskovits, and G. A. Ozin, *Angew. Chem., Int. Ed. Engl.*, **14**, 292 (1975), and references therein.

(11) R. Busby, W. Klotzbücher, and G. A. Ozin, *J. Am. Chem. Soc.*, **98**, 4013 (1976).

(12) T. A. Ford, E. P. Kündig, W. Klotzbücher, M. Moskovits, and G. A. Ozin, *J. Chem. Phys.*, **66**, 524 (1977).

(13) (a) T. C. DeVore, A. Ewing, H. F. Franzen, and V. Calder, *Chem. Phys. Lett.*, **35**, 78 (1975); (b) H. Huber, G. A. Ozin, and W. J. Power, *J. Am. Chem. Soc.*, **98**, 6508 (1976); (c) J. Hulse and M. Moskovits, *J. Chem. Phys.*, **66**, 3988 (1977).

(14) E. P. Kündig, M. Moskovits, and G. A. Ozin, *J. Am. Chem. Soc.*, **97**, 2097 (1975); G. A. Ozin, *Appl. Spectrosc.*, **30**, 573 (1976).

(15) W. Klotzbücher and G. A. Ozin, *Inorg. Chem.*, **16**, 984 (1977).

(16) C. Moore, *Natl. Bur. Stand. (U.S.), Monogr.*, **No. 53** (1962).

(17) J. M. Brom, Jr., W. R. M. Graham, and W. Weltner, Jr., *J. Chem. Phys.*, **57**, 4116 (1972).

(18) D. M. Mann and H. P. Broida, *J. Chem. Phys.*, **55**, 84 (1971); L. Brewer and C. Chang, *ibid.*, **56** (1972); D. M. Green and D. H. W. Carstens, *ibid.*, **54**, 5206 (1971); W. Klotzbücher and G. A. Ozin, *Inorg. Chem.*, **15**, 292 (1976); D. H. W. Carstens, W. Brashear, D. R. Eslinger, and D. M. Gruen, *Appl. Spectrosc.*, **26**, 184 (1972). See D. M. Gruen in "Cryochemistry", M. Moskovits and G. A. Ozin, Ed., Wiley, New York, N.Y., 1976, for detailed discussions of "matrix-induced frequency shifts".

(19) W. F. Cooper, G. A. Clarke, and C. R. Hare, *J. Phys. Chem.*, **76**, 2268 (1972); P. Joyes and M. Leleyter, *J. Phys. B*, **6**, 150 (1973); R. P. Messmer, S. K. Knudson, K. H. Johnson, J. B. Diamond, and C. Y. Yang, *Phys. Rev. B*, **13**, 1396 (1976); C. F. Melius, J. W. Moskowitz, A. P. Mortola, M. B. Baillie, and M. A. Ratner, *Surf. Sci.*, **54**, 279 (1976); W. A. Goddard III and T. Upton, *J. Am. Chem. Soc.*, in press (and private communication), and references therein.

(20) H. Huber, W. Klotzbücher, G. A. Ozin, and A. Vander Voet, *Can. J. Chem.*, **51**, 2722 (1973).

(21) (a) J. S. Darling, M. B. Garton-Sprenger, and J. S. Ogden, *Faraday Soc. Symp.*, **8**, 75 (1973). (b) Note that a detailed electronic spectral examination of binary $M(O_2)_2$ complexes (M = Ti, V, Cr, Mn, Fe, Co, Ni, Cu) indicate that an end-on superoxide formulation might be more appropriate: H. B. Gray, A. B. P. Lever, and G. A. Ozin, in preparation.

(22) L. Vaska, *Acc. Chem. Res.*, **9**, 175 (1976).

(23) L. Andrews, *J. Mol. Spectrosc.*, **61**, 337 (1976), and references therein.

(24) M. A. Bennett and P. A. Longstaff, *J. Am. Chem. Soc.*, **91**, 6266 (1969), and C. Masters and B. L. Shaw, *J. Chem. Soc. A*, 3678 (1971).

(25) See for example W. Klotzbücher and G. A. Ozin, *Inorg. Chem.*, **15**, 292 (1976).

(26) G. A. Ozin and A. Vander Voet, *Can. J. Chem.*, **51**, 3332 (1973).

(27) W. Klotzbücher and G. A. Ozin, *J. Am. Chem. Soc.*, **97**, 3765 (1975).

(28) Trace impurities can originate from (i) the walls of the vacuum system, (ii) the matrix gases themselves, (iii) small air leaks in the vacuum system, and (iv) the trace carbon content of the metal vapor source reacting with trace amounts of dioxygen to yield CO and/or CO_2.

(29) W. Klotzbücher, G. A. Ozin, J. G. Norman, Jr., and H. Kolari, *Inorg. Chem.*, **16**, 2871 (1977).

(30) W. Klotzbücher and G. A. Ozin, *J. Mol. Catal.*, in press, and paper presented at the meeting "Relationships between Homogeneous and Heterogeneous Catalysis", Lyon, Nov 1977.

(31) H. Huber and G. A. Ozin, *Inorg. Chem.*, in press, and paper presented at the meeting "Matrix Isolation Spectroscopy", West Berlin, June 1977; W. Schulze, H. U. Becker, and H. Abe, paper presented at the same conference.

Contribution from the Lash Miller Chemistry Laboratory and Erindale College, University of Toronto, Toronto, Ontario, Canada

Rhodium Atom Chemistry. 2. Interaction of Small, Well-Defined Rhodium Clusters with Dioxygen. $Rh_2(O_2)_n$ and $Rh_3(O_2)_m$, Localized Bonding Models for Dioxygen Chemisorption on Rhodium Metal

A. J. LEE HANLAN and GEOFFREY A. OZIN*

Received January 11, 1977 AIC70012I

The interaction of small, well-defined rhodium clusters, Rh_n (where $n = 2$ or 3), with molecular dioxygen has been investigated for the first time by matrix infrared and UV–visible spectroscopy coupled with metal/dioxygen concentration experiments, warmup studies, and dioxygen isotopic substitution techniques. A number of binuclear dioxygen complexes of the type $Rh_2(O_2)_n$ (where $n = 1, 2, 3$, or 4) together with a trinuclear $Rh_3(O_2)_m$ (where m is probably 2 or 6) have been identified and characterized spectroscopically. The properties of these complexes are most intriguing. $Rh_2(O_2)_4$, for example, can be considered to be the metal–metal bonded dimer of the parent monomer $Rh(O_2)_2$, the latter having been defined in part 1 of this study. Moreover, the $Rh_2(O_2)_{1-3}$ reactive intermediates can be visualized as being derived from $Rh_2(O_2)_4$ by successive dioxygen stripping. It would also appear that the highest stoichiometry trimer complex $Rh_3(O_2)_n$ is also derived from $Rh(O_2)_2$ and is probably best described as a triangular metal cluster of three "$Rh(O_2)_2$" units. In addition to these binuclear and trinuclear cluster compounds containing dioxygen ligands with oxygen–oxygen stretching frequencies in the range normally expected for coordinated $O_2^{\delta-}$ (ν(OO) 1150–850 cm^{-1} for $1 \leq \delta \leq 2$), there also exists a fascinating binuclear $Rh_2(O_2)$ complex which exhibits an unprecedentedly high oxygen–oxygen stretching mode at 1275–1265 cm^{-1}. All of the cluster complexes described, together with their mononuclear counterpart complexes $Rh(O_2)_{1,2}$, are considered in this paper to be useful localized bonding models for probing the chemisorbed state of dioxygen on rhodium metal surfaces and are discussed in terms of their possible relevance to some heterogeneous oxidation catalysis involving olefins.

Introduction

The past decade has witnessed a renaissance in surface crystallography and surface spectroscopy to the point that reliable microscopic information is almost becoming routinely available on the interaction between transition metal surfaces and a variety of atoms and molecules.[1a] In both theoretical[1b] and experimental[1c] studies of chemisorption and catalysis, a great deal of discussion has focused on the validity of em-